九州大学大学院総合理工学報告
第 46 巻 第 2 号 6-10 頁 令和 7 年 2 月

Engineering Sciences Reports, Kyushu University
Vol. 46, No. 2, pp. 6-10, FEB, 2025

High-resolution three-dimensional visualization of dislocations in Mo using weak-beam dark-field electron tomography

Yifang ZHAO,[*1†] Hirotaka SAKAI,[*2] Hikaru SAITO,[*3] and Satoshi HATA[*4]

[†]E-mail of the corresponding author: zhao.yifang.918@s.kyushu-u.ac.jp

(Received December 25, 2024, accepted January 16, 2025)

This study improved the data quality and spatial resolution of dislocation tomography using weak-beam dark-field (WBDF)- scanning transmission electron microscopy (STEM) by increasing the beam current and applying image processing. The 3D visualization of dislocation structures in a single crystal Mo was compared with results obtained under the conventional strong-beam bright-field (SBBF) imaging condition. The results showed that WBDF-STEM provided higher dislocation intensity in tilt series and achieved a 17% higher spatial resolution in 3D reconstruction results compared to SBBF-STEM. These findings demonstrate that the improved WBDF-STEM effectively extends the advantages of WBDF 2D imaging to 3D dislocation observation, establishing its potential as a powerful tool for characterizing dislocation structures in crystalline materials.

Key words: *Scanning transmission electron microscopy, Electron tomography, Three-dimensional (3D), Dislocations.*

1. Introduction

Dislocations, a common type of line crystal defects, significantly influence the mechanical properties of crystalline materials. Dislocations often exhibit complex arrangements and morphologies. Conventional observation methods used to study dislocations, such as transmission electron microscopy (TEM) and scanning transmission electron microscopy (STEM), reveal only the projection of dislocation viewed from one direction. Therefore, a method for characterizing dislocations' three-dimensional (3D) structure is required. Since pioneering work by Barnard et al.[1], electron tomography (ET) has become one of the conventional techniques for 3D observation of dislocations in crystalline materials[2-4]. In their work, a dataset of weak-beam dark-field (WBDF)[5] images (referred to as tilt series) was acquired using TEM every few degrees over a specimen tilt range of ±60° while ensuring that the used reciprocal lattice vector was parallel to the tilt axis so that the diffraction condition was constant through the data acquisition.

Compared to conventional strong-beam (or two-beam) conditions using fundamental diffractions $\boldsymbol{g}$, WBDF conditions employ higher-order diffractions with a larger deviation vector $\boldsymbol{s}$, such as $3\boldsymbol{g}$ and $4\boldsymbol{g}$, can provide higher dislocation image intensity. The dislocation lines appear narrower and are closer to the actual position of the dislocation cores in the WBDF images. This is because at a larger $\boldsymbol{s}$, only larger lattice distortions can satisfy the Bragg's condition. Since the lattice distortions increase closer to the dislocation cores, only the area close to the dislocation cores is imaged in the WBDF images. The distance $\boldsymbol{r}$ between the dislocation line and the actual position of the dislocation core can be described as[1, 5, 6]:

$$\boldsymbol{r} \propto \frac{\boldsymbol{g} \cdot \boldsymbol{b}}{2\pi \boldsymbol{s}} \tag{1}$$

*1 Department of Interdisciplinary Engineering Sciences, Graduate Student
*2 Department of Applied Science for Electronics and Materials, Graduate Student
*3 Institute for Materials Chemistry and Engineering
*4 Department of Advanced Materials Science and Engineering

and the dislocation line width $\boldsymbol{x}$ can be described as[5, 6]:

$$\boldsymbol{x} \propto \frac{1}{\pi \boldsymbol{s}} \quad (2)$$

Therefore, the larger $\boldsymbol{s}$ is, the closer the dislocation line is to the actual position of the dislocation core, and the narrower the dislocation line width. Additionally, the images obtained under WBDF conditions with a larger $\boldsymbol{s}$ can reduce the effects of the dynamical diffraction and minimize interference from the elastic strain field background surrounding dislocations, providing higher dislocation image intensity[1, 5, 6]. These advantages of WBDF conditions can be used to visualize dislocations with high resolution and image intensity. However, using large $\boldsymbol{s}$ for imaging also leads to a lower signal-to-noise ratio (S/N). In the dislocation tomography, the rapid decrease in S/N in WBDF images at high specimen tilt angles makes it easier to break the projection requirement[7, 8], resulting in WBDF-ET typically requiring image processing or is conducted at smaller specimen tilt range[1, 9, 10].

Furthermore, compared to TEM-ET, STEM-ET has also improved data quality in terms of dislocation intensity (e.g., Ref. 11), where strong-beam (SB) conditions have been chosen. Indeed, the STEM has an advantage in avoiding chromatic aberration when observing thick specimens, as demonstrated by a successful reconstruction of dislocation arrangement in an α-Fe specimen with a 300~400 nm thick by a 300 kV electron microscope[12, 13]. As suggested in Ref. 12, the SB conditions are not always the best choice for dislocation tomography especially regarding spatial resolution. The WBDF-STEM has the potential to improve dislocation tomography.

In this study, we improved the S/N ratio of WBDF-STEM for dislocation tomography by increasing the beam current and applying image processing. We examined how WBDF-STEM improves data quality for 3D reconstruction compared to the conventional SB-STEM condition by obtaining the two datasets of tilt series for the same dislocations in a Mo foil specimen. As a result, the improved WBDF-STEM provides higher spatial resolution than SB-STEM in dislocation tomography.

2. Experimental

A single crystal Mo was used as the specimen. The specimen was cut into square sheets of 1.5 mm × 1.5 mm × 0.05 mm in size and then ion-milled to prepare a thin foil specimen for STEM observation.

Table 1 The conditions for tilt series acquisition.

Specimen tilt step [degree]	1 (−70 to −50, +50 to +70), 2 (−50 to +50)
Diffraction condition	$\boldsymbol{g}$/3$\boldsymbol{g}$ for WBDF, and two-beam condition $\boldsymbol{g}$ for SBBF, $\boldsymbol{g}$ = 200
Image size [pixel]	1024 × 1024
Scan speed [μs/pixel]	5
Beam current [nA]	0.2 (SBBF), 2(WBDF)

A Titan Cubed G2 TEM/STEM (Thermo Fisher Scientific Inc.) was operated at an acceleration voltage of 300 kV, under the parallel-beam STEM mode with a 1.20 mrad convergence semi-angle of the incident electron beam. The camera length was set to 230 mm. A bright-field (BF) STEM detector detected transmitted electrons with a scattering angle range of 0–5 mrad. Dislocations were observed under the WBDF condition and SBBF condition, respectively. The diffraction conditions were managed using a high-angle triple-axis (HATA) specimen holder[14] (Mel-Build Inc.) through a specimen tilt range of ±70°. The acquisition conditions for the tilt series are shown in Table 1.

The Gaussian adaptive thresholding was performed to binarize the acquired tilt series datasets, aiming to eliminate the influence of specimen thickness variations on dislocation contrast during specimen tilting[13]. The same binarization parameters were used for both tilt series datasets to avoid the influence of the binarization process on the evaluation of the 3D reconstruction results.

The Composer™ software (SYSTEM IN FRONTIER INC.) was used to align the tilt series and reconstruct 3D volumes of the object by the simultaneous iterative reconstruction technique (SIRT) with 20 times iterations. The Visualizer-evo™ software (SYSTEM IN FRONTIER INC.) was then used for visualizing the reconstructed 3D volumes.

3. Results and discussion

3.1 The tilt series images

Fig. 1 shows a portion of the tilt series (91

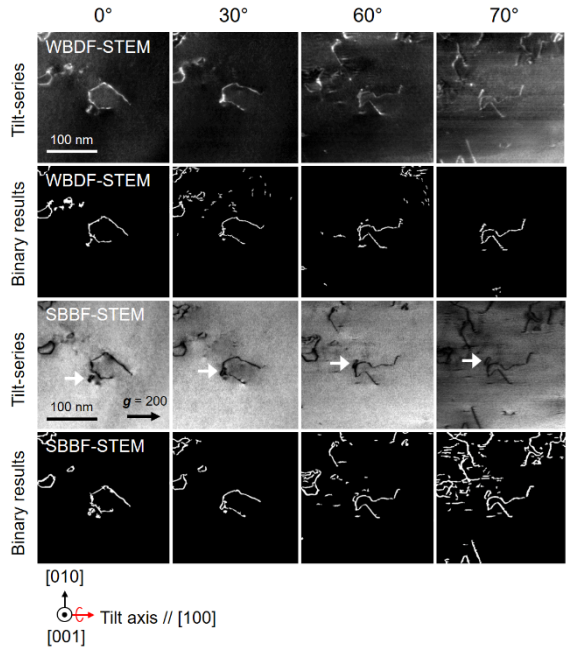

Fig.1 Images at 0°, 30°, 60° and 70° tilt angles from the tilt-series obtained using WBDF- and SBBF-STEM under the same field of view and their binary results. The dislocation loop is indicated by the white arrows.

images each) obtained using WBDF- and SBBF-STEM at the same field of view and their binarization results. Some typical dislocations and dislocation loops (e.g., indicated by white arrows) are observed in the field of view. These dislocation loops were introduced by possibly ion-milling for the thin-foil specimen preparation. Due to the enhanced beam current used in WBDF-STEM, no significant noise was observed in the WBDF-STEM tilt-series images up to a specimen tilt angle of 60°, and the dislocation intensity remained constant without significant changes. The image quality of the WBDF-STEM tilt-series was comparable to that of the SBBF-STEM tilt-series. At higher tilt angles (e.g., 70°), stripe-shaped noise appeared, and dislocation intensity decreased in both WBDF-STEM and SBBF-STEM images. This is due to the increased electron beam penetration lengths, which reduces the electron transmittance and consequently lowers the image quality. The binarization processing eliminated most of the noise and kept the dislocation intensity constant in the tilt series.

To quantitatively evaluate the differences in dislocation intensity between WBDF-STEM and SBBF-STEM images, the dislocation intensities in the two tilt series were measured. Taking Fig. 2(a, b) as an example, Fig. 2(b) shows the local intensity profile along the

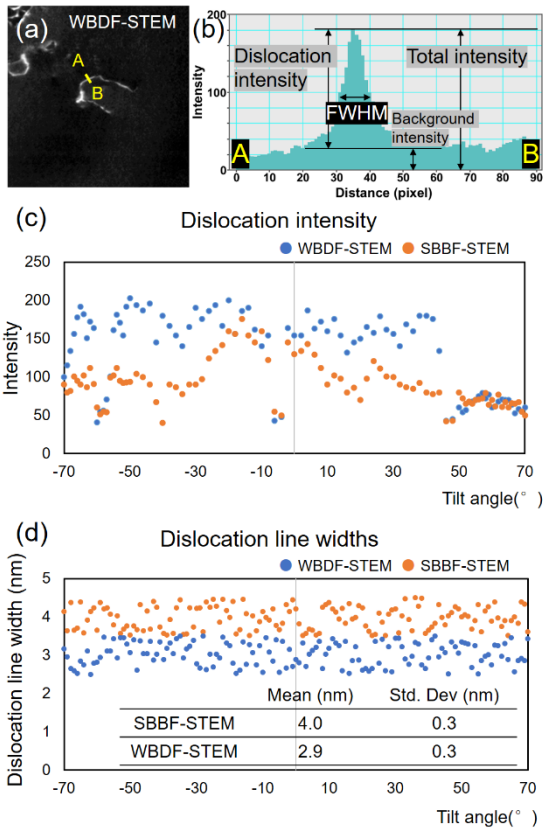

Fig.2 (a) An image from the WBDF-STEM tilt series. The local intensity histogram along the yellow line, A-B, is shown in (b). The dislocation intensity is defined as the total intensity minus the background intensity. (c) The result of measuring the dislocation intensities at ten points with an equal distance apart on each image of the tilt series and calculating the average value. (d) The result of measuring the dislocation line widths at ten positions with an equal distance apart on each image of the tilt series and calculating the average value.

yellow line, A-B, in Fig. 2(a). The dislocation intensity is defined as the total intensity minus the background intensity. The dislocation intensities of ten positions were measured at equal distances apart on each image of the tilt series and the average value was calculated. The results are shown in Fig. 2(c). The two sets of tilt series show similar dislocation intensities around 0°. Overall, the dislocation intensity in the WBDF-STEM images is higher than that in the SBBF-STEM images. Specifically, when the specimen was tilted from -30° to -70°, and from 10° to 50°, the dislocation intensity decreased from ~150 to less than 100 in the SBBF-STEM images but maintained a higher value of 150 to 200 in the WBDF-STEM images. Even though the dislocation intensity in the WBDF-STEM

image decreased rapidly at high tilt angles from 50° to 70°, it was maintained at a value comparable to that of SBBF-STEM.

In addition, the dislocation line widths in the tilt series were measured using the full-width at half maximum (FWHM) of the dislocation intensity. The results are shown in Fig. 2(d). The dislocation line widths in the two tilt series appear to be unaffected by specimen tilt. The mean value of 2.9 nm for WBDF-STEM is slightly lower than that of 4.0 nm for SBBF-STEM, suggesting that the WBDF-STEM imaging shows a higher spatial resolution in dislocation observation compared to the SBBF-STEM imaging.

These results suggest that increasing the beam current of WBDF-STEM can improve the issue of low image quality at high tilt angles over 50° in WBDF-ET. The improved WBDF-STEM can enhance the advantages of WBDF for 3D observation of dislocations. The improved WBDF-STEM can also provide comparable or even better image quality in tilt series than the SBBF-STEM.

3.2 3D reconstruction results

Fig. 3 shows the 3D reconstruction results using the binarized WBDF-/SBBF-STEM tilt series. A 3D reconstruction volume of 400 × 400 × 200 pixels rotated 0°, 30°, 70° and 90° around the x-axis. The 3D image reconstructed from the WBDF-STEM tilt series shows a dislocation that is not observed in the 3D image reconstructed from the SBBF-STEM tilt series, which is indicated by white arrows. By examining the WBDF-STEM tilt series, we found that this difference is due to the change in dislocation morphology during the acquisition of the tilt series. As shown in Fig. 4, the dislocations indicated by the white arrows

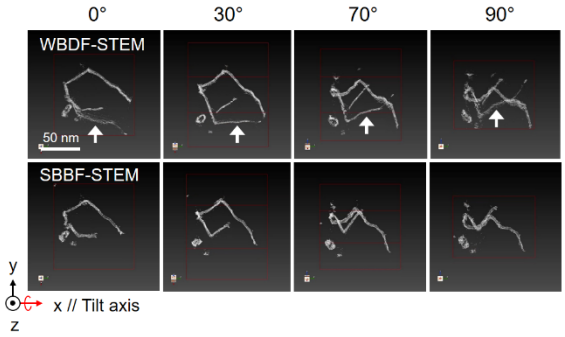

Fig.3 The 3D reconstruction results using the binarized WBDF-/SBBF-STEM tilt series. The white arrow indicates a dislocation in the WBDF-STEM images but invisible in the SBBF-STEM images.

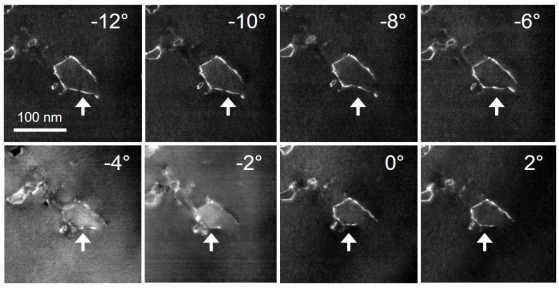

Fig.4 WBDF-STEM tilt series images of a tilt angle between -12° and 2°. White arrows indicate dislocations with morphological changes.

changed its length as the specimen was tilted from -10° to -2°. From the images acquired before and after this tilt range, it is evident that this morphological change in the dislocations is not due to a change in the observation direction. Several reports suggested that dislocation loops in Mo single crystals may creep or interact with surrounding dislocations during irradiation at room or high temperatures[15, 16]. In this study, the acquisition time for WBDF-STEM ranged from 2 to 5 minutes per image, requiring several hours to acquire the tilt series dataset. Considering that the improved WBDF-STEM uses a beam current of 2 nA to increase the electron dose, we considered that the observed morphological changes in dislocations are due to irradiation creep of the dislocations induced by prolonged irradiation with electron beam exposure. It is expected that the other 3D reconstruction methods that require only a few tilt series images, such as the iterative-series reduction (ISER) algorithm[17], could minimize electron beam-induced effects. The evaluation of the 3D reconstruction results will be performed where the dislocation morphology remains unchanged.

We evaluated the spatial resolution of the 3D reconstruction results from WBDF-STEM and SBBF-STEM by measuring the cross-sectional area of the 3D reconstruction volume. Taking Fig. 5(a, b) as an example, a slice was extracted along the x-axis in Fig. 5(a), resulting in the cross-sectional view shown in Fig. 5(b). The dislocation cross-section in the slice can be seen as a rectangle with an area of $\boldsymbol{ab}$. The smaller the area of the rectangle, the higher the spatial resolution. The results of the dislocation cross-sectional area measurements from 400 slices along the x-axis are shown in Fig. 5(c).

According to the results, the average value of the cross-section area for the case of WBDF-STEM (45.7 nm²) is approximately 17% smaller

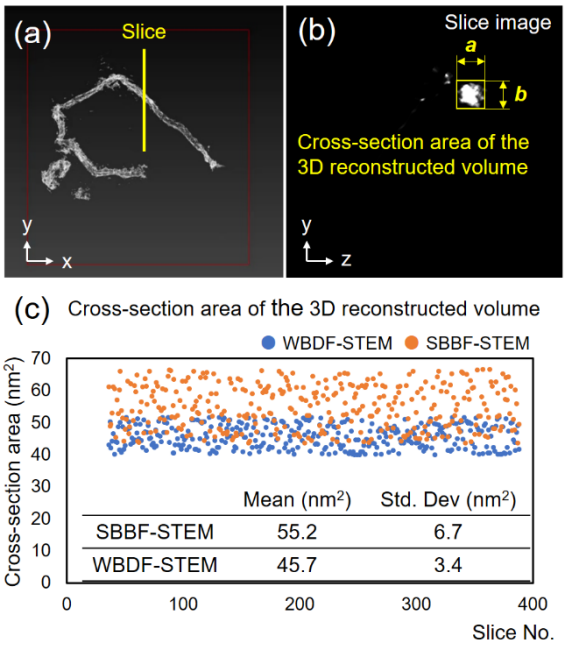

Fig.5 (a) A dislocation image reconstructed from the SBBF-STEM tilt series. Here, a slice is extracted along the x-axis resulting in the cross-section view shown in (b). The dislocation cross-section in the slice can be seen as a rectangle with an area of ***ab***. (c) The results of the dislocation cross-section area measurements from 400 slices along the x-axis.

than that for the case of SBBF-STEM (55.2 nm²). This indicates that WBDF-STEM offers a superior spatial resolution in 3D reconstruction. Moreover, the smaller standard deviation observed in WBDF-STEM can be attributed to the dislocation lines in 2D images being closer to the actual positions of the dislocation cores. As a result, the 3D reconstructed intensity distribution of dislocation lines is more concentrated around the dislocation cores in the 3D reconstruction. These advantages make the ring-like structure of the dislocation loop in Fig. 4 more easily identified in the WBDF-STEM images than in the SBBF-STEM images.

4. Summary and Conclusion

This study improved the data quality and spatial resolution of dislocation tomography using WBDF-STEM by increasing the beam current and applying image processing. The 3D visualization of dislocation structures in a single crystal Mo was compared with results obtained under conventional SBBF conditions. The following conclusions are drawn:

1. Increasing the beam current and applying binarization processing effectively reduced noise in the tilt series, preserving the high spatial resolution advantage of WBDF in 2D dislocation observation.
2. Compared to conventional SBBF-STEM, the improved WBDF-STEM demonstrated higher dislocation intensity in the tilt series, especially at tilt angles of 30° to 50°.
3. The spatial resolution of 3D reconstructions using WBDF-STEM was approximately 17% higher than that for SBBF-STEM, suggesting that the reconstructed dislocation volume is located closer to the actual position of the dislocation core.
4. Prolonged electron beam exposure may influence dislocation structures, which could be avoided by improving the 3D reconstruction algorithm.

The improved WBDF-STEM imaging method enhances the data quality of dislocation tomography. This advancement demonstrates the potential of WBDF-STEM as a powerful tool for the characterization of dislocation structures in crystalline materials.

Acknowledgments

This work was partly supported by JST SPRING (Grant Numbers JPMJSP2136).

References

1) J. S. Barnard et al., Philos. Mag., 86, 4901 (2006).
2) M. Tanaka et al., Scripta Mater. 59, 901 (2008).
3) J. P. Kacher et al., Scripta Mater. 64, 677 (2011).
4) G. S. Liu et al., Mater. Charact. 87, 1 (2014).
5) D. J. H. Cockayne, Z. Naturforsch. A. 27, 452 (1972).
6) D. B. Williams et al., "Imaging in the TEM." Transmission Electron Microscopy: A Textbook for Materials Science (1996) p349.
7) P. W. Hawkes, "The electron microscope as a structure projector" in "Electron tomography: three-dimensional imaging with the transmission electron microscope", ed. by J. Frank, Boston, Springer US, (1992) p.17.
8) P. A. Midgley et al., Ultramicroscopy 96, 413 (2003).
9) G. S. Liu et al., J. Mater. Res. 26, 514 (2011).
10) Z. Q. Feng et al., Curr. Opin. Solid State Mater. Sci. 24, 100833 (2020).
11) M. Tanaka et al., Mater. Trans. 49, 1953 (2008).
12) K. L. Hasezaki et al., Ultramicroscopy 182, 249 (2017).
13) Y. F. Zhao et al., Sci. Rep. 11, 20720 (2021).
14) S. Hata et al., Ultramicroscopy 111, 1168 (2011).
15) C. A. English et al., Philos. Mag.-J. Theor. Exp. Appl. Phys. 35, 533 (1977).
16) Y. Li et al., Acta Mater. 201, 462 (2020).
17) H. Kudo et al., Kenbikyo (in Japanese) 51, 48 (2016).